Overview of the High-Level Trigger Electron and Photon Selection for the ATLAS Experiment at the LHC

S. Armstrong*, J.T.M. Baines†, P. Casado‡, A. Clark‖, P. Conde-Muiño§, D. Damazio*, A. De Santo¶, M. Diaz Gomez‖, D. Emeliyanov†, O. Gaumer‖, S. George¶, R. Gonçalo¶, A. Khomich**, G. Kilvington¶, N. Konstantinidis††, A. Kootz‡‡, A. Lowe¶, T. McMahon¶, A.G. Mello[x], C. Osuna‡, C. Padilla§, F. Parodi[xi], V. Perez Reale[xii], K. Pretzl[xii], C. Santamarina§, C. Schiavi[xi], S. Sivoklokov[xiii], E. Stefanidis††, M. Sutton††, E. Thomas[xii], P. Teixeira-Dias¶, A. Watson[xiv], M. Wielers†, E. Woehring[xiv], X. Wu‖ *Brookhaven National Laboratory (BNL), Upton, New York, USA †Rutherford Appleton Laboratory, Chilton, Didcot, UK ‡Institut de Física d'Altes Energies (IFAE), Universidad Autónoma de Barcelona, Barcelona, Spain §CERN, Genève, Switzerland ¶Department of Physics, Royal Holloway, University of London, Egham, UK ‖Section de Physique, Université de Genève, Switzerland **Lehrstuhl für Informatik V, Universität Mannheim, Mannheim, Germany ††Department of Physics and Astronomy, University College London, London, UK ‡‡Fachbereich Physik, Bergische Universität Wuppertal, Germany [x]Universidade Federal do Rio de Janeiro, COPPE/EE, Rio de Janeiro, Brazil [xi]Dipartimento di Fisica dell'Università di Genova e I.N.F.N., Genoa, Italy [xii]Laboratory for High Energy Physics, University of Bern, Switzerland [xiii]Institute of Nuclear Physics, Moscow State University, Moscow, Russia [xiv]University of Birmingham, Birmingham, UK

Presented by R. Gonçalo, Royal Holloway, University of London, London, UK

ATL-DAQ-CONF-2005-036
05 December 2005

***Abstract*— The ATLAS experiment is one of two general purpose experiments to start running at the Large Hadron Collider in 2007. The short bunch crossing period of 25 ns and the large background of soft-scattering events overlapped in each bunch crossing pose serious challenges that the ATLAS trigger must overcome in order to efficiently select interesting events. The ATLAS trigger consists of a hardware-based First-Level Trigger and of a software-based High-Level Trigger, which can be further divided into the Second-Level Trigger and the Event Filter. This paper presents the current state of development of methods to be used in the High-Level Trigger to select events containing electrons or photons with high transverse momentum. The performance of these methods is presented, resulting from both simulation studies, timing measurements, and test beam studies.**

***Index Terms*— ATLAS, LHC, trigger, electron, photon.**

I. Introduction

THE ATLAS experiment is one of two general-purpose experiments currently being built at the Large Hadron Collider (LHC). The LHC will push the high-energy frontier in collider experiments to new, as yet unexplored regions. Along with the highest centre of mass energy ever attained with colliding beams, the bunch-crossing period will also be extremely short (25 ns). In addition, ~ 23 soft proton-proton interactions will be overlapped in each bunch crossing at design luminosity ($10^{34} cm^{-2} s^{-1}$). This creates a challenging environment in which to select hard-scattering events against a very high background of soft QCD events. The trigger output rate will be limited to $\sim 200 Hz$, which means that the ATLAS trigger will aim to select around five events for every million bunch crossings.

The ATLAS trigger is naturally divided into the First-Level Trigger [1] (LVL1), which runs in dedicated hardware, and the software-based High-Level Trigger [2] (HLT), which will run on a computer farm. The High-Level Trigger is further subdivided into level 2 (LVL2) and the Event Filter (EF). This paper focuses on the operation of the HLT and its performance in selecting events containing high transverse momentum electrons or photons.

II. The ATLAS detector

The ATLAS detector is described in detail elsewhere [3]. It is composed (from the centre of the detector outwards) of the inner tracking detector [4] (ID); a thin superconducting solenoid, generating a magnetic field of 2 T; a liquid argon-lead electromagnetic calorimeter [5] (LAr) separated into barrel and endcap sections; an hadronic calorimeter (Tile, HEC and FCAL); and a muon spectrometer system [6] (Muon). The ATLAS detector effectively covers the angular region[1] corresponding to $|\eta| < 2.5$ for tracking and $|\eta| < 4.9$ for calorimetry (with the electromagnetic calorimeter extending up to $|\eta| < 3.2$).

As the ID and the LAr are relevant to the electron and photon triggers discussed in this paper, a more thorough description of these detector systems is given here.

[1]The pseudorapidity, η, is defined as $\eta = -\log \tan \theta/2$, where θ is the polar angle defined with respect to the beam direction.

The ID tracking detectors consist of a three-layer[2] semiconductor pixel detector (Pixel) placed near to the interaction point; a semiconductor strip detector (SCT); and a transition radiation tracker (TRT) composed of straw-tube proportional chambers interspersed with a radiator material.

The LAr electromagnetic calorimeter lead absorber has an accordion geometry which results in a very good spatial uniformity with respect to the azimuthal angle, ϕ, and is divided into three longitudinal samplings. It is expected to achieve an energy resolution [3] given by $\sigma_E/E = 10\%/\sqrt{E} \oplus 0.7\% \oplus 0.27\%/E$. where E is the energy expressed in GeV.

III. The ATLAS trigger

This section gives a brief description of the ATLAS trigger system. Further details can be found elsewhere [3].

A. Level 1

The primary task of LVL1 is to perform a preliminary rejection of background, in order to reduce the 40 MHz input rate, which corresponds to the bunch crossing rate, to less than around 75 kHz (upgradable to 100 kHz). It uses (coarse granularity) data from the calorimeter and muon detector systems, but not from Inner Detector tracking chambers. LVL1 must reach a decision within $2.2\mu s$. For accepted events, in which a certain signature is satisfied (e.g. an electromagnetic cluster is found in the LAr), LVL1 passes to LVL2 the location of the identified objects.

At LVL1, calorimeter information is available with the granularity of trigger towers. These are approximately projective groups of cells with the approximate size $\Delta\eta \times \Delta\phi = 0.1 \times 0.1$.

Candidate electromagnetic clusters are identified, at this trigger level, by the energy deposited in a set of 2×2 LAr trigger towers. The cluster transverse energy, E_T is measured in the set of 2×1 or 1×2 towers with the highest energy. The 12 LAr towers surrounding the cluster are used to test the cluster isolation. The 16 trigger towers behind the electromagnetic cluster and the isolation ring are used to determine the cluster isolation in the hadronic calorimeter (leakage).

B. Level 2

Level 2 can access event data from all the ATLAS subdetectors with the full detector granularity. On the other hand, the available time is not sufficient for a full event reconstruction. Instead, LVL2 retrieves detector data only from the regions where LVL1 has found interesting objects. These regions are known as Regions of Interest (RoI) and correspond to $\sim 2\%$ of the event size ($\sim 1.5MB$). On average, 1.4 RoIs are found per event [2].

Within each RoI, LVL2 can reconstruct physics objects such as charged tracks and calorimeter showers using fast tracking and calorimetry algorithms. When an event is accepted by LVL2, a summary of the LVL2 processing is appended to the event stream which is passed to the Event Filter. The average time available for processing at LVL2 is 10 ms. The expected output rate is around 1 kHz. It should be noted here that this is not a hard limit. Instead, it is an estimated time based on the expected number of processors running on the LVL2 CPU farm. The 10 ms benchmark relates to 8 GHz processors or equivalent multi-core processors running at lower clock speeds. It is expected that 500 8 GHz-equivalent multi-core processors will be used in the LVL2 farm [7].

[2]Only two layers are expected to be present for the initial running period.

C. The Event Filter

The Event Filter has, like LVL2, access to event data with full granularity. The RoI mechanism is also used at the EF and is seeded by LVL2. The Event Filter has, on average, one second to process each event (on 8 GHz processors or equivalent multi-core processors). This allows the use of more sophisticated algorithms at the EF than is possible at LVL2. One example of this is that the EF runs offline reconstruction algorithms and is expected to apply calibration and alignment corrections as in the offline event reconstruction[3]. This strategy also avoids the duplication of software development work and simplifies software maintenance.

D. HLT steering

The HLT operation aims to reject background events as early as possible, to optimize the usage of available resources. To do this, the operation of each of LVL2 and EF for a given signature is broken down into reconstruction algorithms interspersed with hypothesis-testing algorithms. As soon as an hypothesis algorithm in a trigger signature fails, the signature is abandoned for the current RoI, and the available resources become free to be used by other signatures [8].

IV. The HLT electron and photon selection

At LVL2, calorimeter data in the RoIs is retrieved from the calorimeter readout buffers. A fast clustering algorithm [9] runs on this data and calculates several quantities which characterize the electromagnetic shower:

- $R_{shape} = E_{3\times7}/E_{7\times7}$: the ratio of the energy deposited in sampling 2 of the LAr (granularity $\Delta\eta \times \Delta\phi = 0.025 \times 0.025$) in a set of 3×7 cells to that deposited in 7×7 cells. This variable is close to unity for electron showers;
- $R_{strips} = (E_1 - E_2)/(E_1 + E_2)$ where E_1 and E_2 are the energies read in the first sampling cells (known as strips, $\Delta\eta \times \Delta\phi = 0.003 \times 0.1$ in the barrel) with the highest and second highest energy readings in the cluster. This variable is most discriminant against $\pi^0 \to \gamma\gamma$ decays and is close to one for single electron or photon clusters;
- E_T^{em}: the transverse energy deposited in the all samplings of the LAr in the angular region corresponding to 3×7 cells in sampling 2;

[3]Although the accuracy of this alignment and calibration will be better for offline reconstruction, especially for reconstruction of data in reprocessings.

- E_T^{had}: the total transverse energy deposit in the hadronic calorimeter within the LVL1 RoI (leakage).

A hypothesis-testing algorithm then applies cuts on the cluster parameters, to reject clusters produced by jets or photons from π^0 decay. In the case of the photon signatures, tighter cuts are applied to the electromagnetic cluster, as these signatures must rely solely on calorimeter quantities.

In the case of electron signatures, further discrimination is achieved by using information from the inner detector. Charged tracks can be reconstructed at LVL2 using inner detector data from the RoI and fast tracking algorithms [10], [11].

If a charged track is found in the RoI above a given threshold of transverse momentum the track is matched to the calorimeter cluster by applying cuts on the following quantities:

- $\Delta\eta_{trk}^{cluster}$ and $\Delta\phi_{trk}^{cluster}$: separation in η and ϕ between the track extrapolated to the calorimeter face and the electromagnetic cluster;
- E_T/p_T: ratio between the cluster transverse energy, E_T, and the track transverse momentum, p_T.

At the Event Filter, a similar sequence of algorithms is run. Offline algorithms are employed at this trigger level with little modification [12], together with offline-like calibration and alignment. In addition to a better accuracy of the reconstruction, due to the use of offline reconstruction algorithms, more sophisticated cuts are also possible, such as quality cuts on reconstructed charged tracks found in the inner detector. It should also be noted that the position of the RoI is updated with increasing precision by each HLT reconstruction algorithm.

V. Performance studies

This section describes several studies performed on the electron and photon signatures at the HLT.

A note should be made at this point on the naming of trigger signatures. The ATLAS convention for signature names usually contains the physical object(s) that the signature corresponds to, the transverse momentum at which the signature is efficient, and any additional characteristics. For example: *e25i* is a single electron signature which is efficient for electrons and positrons with transverse momenta above 25 GeV and are found isolated.

A. Single electron signature: e25i

The signature efficiency at the 25 GeV threshold was estimated from a Monte-Carlo simulated sample of single electrons, produced using a realistic description of the ATLAS detector [13] implemented in GEANT4 [14]. The simulated sample also includes electronic noise and the superposition of several proton-proton interactions, corresponding to the initial luminosity scenario of $10^{33}cm^{-2}s^{-1}$. The resulting efficiency values after each processing step are listed in table I. As a function of the pseudorapidity, the signature efficiency drops in the vicinity of the transition between the barrel and endcap calorimeters. This may be attributed to a high amount of inactive material between the interaction point and the calorimeter. This region was excluded from the efficiency calculations.

TABLE I

EFFICIENCIES AND RATES FOR SIGNATURE *e25i* (EXCLUDING BARREL/ENDCAP TRANSITION).

e25i	**Efficiency**	**Rate**
LVL 1	96.7%	$\sim 6\ kHz$
LVL 2 calorimetry	95.2%	$1.2\ kHz$
LVL 2 tracking	88.7%	$450\ Hz$
LVL 2 cluster/track match	88.2%	$240\ Hz$
EF calorimetry	85.4%	$65\ Hz$
EF tracking	81.5%	$43\ Hz$
EF cluster/track match	80.0%	$34\ Hz$

TABLE II

COMPOSITION OF EVENT SAMPLE ACCEPTED BY *e25i*.

$W \to e\nu$	20%
$Z \to e^+e^-$	6%
e from b and c quark decays	8%
γ (quark bremsstrahlung and prompt)	14%
other ($\pi^0 \to \gamma\gamma$, jets, etc)	52%

The overall output rate of this signature was estimated using a Standard Model data sample, simulated with Pythia [15], containing mostly di-jet events, with an admixture of events in which W and Z gauge bosons were produced. The relative fractions of the various types of events are determined by their cross sections. The *e25i* rates after each processing step are listed in table I. It should be noted that the QCD di-jet cross section in the kinematic region under consideration ($p_T^{jet} > 17GeV$) is poorly known. The corresponding uncertainty in the trigger rates may be as high as a factor of two to three.

Using the Standard Model data sample, the composition of the events selected by this signature can studied. This is listed in table II. In a large fraction of events, the electron signature is faked by other particles such as converted photons from various sources or hadronic jets. In around a third of the events, on the other hand, high-p_T electrons are present and can trigger the event.

B. Trigger cuts optimization

The cuts applied in the HLT can be tuned to obtain the maximum possible efficiency for a certain trigger rate, or equivalently, for a certain value of the background rejection ratio. This ratio is defined here as the number of background events which is rejected by the trigger, divided by the total size of the background sample. This section describes two methods that are being developed to tune the trigger cuts for each value of efficiency or background rejection.

1) Scanning of cut parameter space: The tuning of the trigger cuts can be done by determining the signal-finding efficiency and the background rejection ratio for several values of each of the cuts applied by the trigger. Figure 1 shows the range of values of efficiency and background rejection achievable at the track-finding step of the LVL2 *e25i* signature. Each point in the plot corresponds to a set of LVL2 tracking cut values. The line visible in the plot shows, in an approximate way, the optimum working region of this trigger step. It corresponds, for

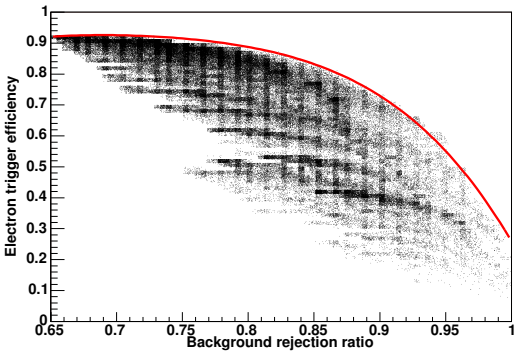

Fig. 1. Efficiency for selecting signal versus background rejection ratio for the LVL2 track-finding step of the *e25i* signature. Each point in the scatter plot corresponds to a set of LVL2 tracking cut values. The line shows, approximately, the optimum working region of this trigger step. It corresponds to the highest achievable background rejection ratio for each value of efficiency.

TABLE III

EFFICIENCIES AND RATES FOR SIGNATURES $2\gamma 20i$ AND $\gamma 60$ AFTER OPTIMIZATION.

Efficiency	$2\gamma 20i$	$\gamma 60$
Level 2	90%	90%
Event Filter	80%	80%
Rate	$2 \pm 1Hz$	$5.8 \pm 0.5Hz$

each value of efficiency, to the highest achievable background rejection.

2) Optimization using simplex method: A second optimization method was developed using signatures *2γ20i* and *γ60*. These correspond to two isolated photons with transverse momentum greater than about 20 GeV and to one photon with transverse momentum greater than about 60 GeV, respectively. In the method described here, the time-consuming sampling of the multidimensional space of signature cuts is optimized by using a minimization algorithm. In the present study, the background rejection ratio was maximized for a certain value of the signal efficiency. A simplex [16] algorithm was used to minimize the function

$$f(k_1,..,k_n) = \frac{e^{|\varepsilon_\gamma(k_1,..,k_n)-X_\varepsilon|}}{\mathcal{R}_B(k_1,..,k_n)} \quad (1)$$

where ε_γ corresponds to the signal efficiency, $\mathcal{R}_B$ is the background rejection ratio, k_i is the i^{th} cut applied by the trigger signature, and X_ε is the value of signal efficiency for which one wants to find the best possible background rejection.

In the present study, values of X_ε of 90% and 80% were used to optimize the *γ20i* signature for LVL2 and EF, respectively. The resulting rates for *2γ20i* and *γ60* are summarized in table III. As the amount of dead material varies as a function of the absolute value of pseudorapidity, the range $|\eta| < 2.5$ was divided into ten regions where the photon trigger thresholds were optimized separately.

TABLE IV

EFFICIENCY OF ELECTRON SIGNATURES FOR SELECTING $Z \to e^+e^-$ AND $W \to e\nu$ EVENTS.

Signature	$Z \to e^+e^-$	$W \to e\nu$
2e15i	67.2%	–
e25i	92.9%	79.6%
e60	20.4%	6.9%
all	94.8%	80.3%

TABLE V

EFFICIENCY OF PHOTON SIGNATURES FOR SELECTING $H \to \gamma\gamma$ EVENTS FOR A STANDARD MODEL HIGGS BOSON WITH $m_H = 120GeV$.

Trigger level	$2\gamma 20i$	$\gamma 60i$	combined
Level 1	94%	85%	98%
Level 2	84%	81%	94%
Event Filter	78%	69%	89%

C. Performance on physics simulated samples

The values reported above refer to the efficiency at the signature thresholds and above. For real physics events, the emitted electrons and photons have a wide range of transverse momenta. The effect of the trigger selection on events containing electrons or photons in the final state was studied for the cases of W and Z gauge boson production. The case of a Standard Model Higgs boson of mass 120 GeV decaying to two photons was also studied. The efficiency values for the relevant electron and photon trigger signatures are shown in tables IV and V.

The efficiency values shown were calculated with events preselected by the following kinematic and angular cuts:

- $Z \to e^+e^-$: two electrons present in the angular range defined by $|\eta| < 2.5$ and with $p_T > 15GeV$;
- $W \to e\nu$: one electron present in the angular range defined by $|\eta| < 2.5$ and with $p_T > 25GeV$;
- $H \to \gamma\gamma$: one photon with $p_T > 40GeV$ and one photon with $p_T > 25GeV$, both within $|\eta| < 2.5$.

In addition, the transition region between the barrel calorimeter and the end-cap was excluded from the calculations.

D. Trigger efficiency estimation from $Z \to e^+e^-$ events

As the trigger efficiency will be an important parameter in several physics analysis, it is important to have several independent methods of estimating it. It is also important to depend as little as possible on the Monte Carlo description of the detector and running conditions, as this is necessarily incomplete. A method to determine the trigger efficiency using $Z \to e^+e^-$ events was developed [17].

The method consists of tagging events using a single-electron signature, such as *e25i*. After offline reconstruction of the events, a sample is selected in which a e^+e^- pair is identified. The e^+e^- invariant mass histogram is then fitted near the Z-boson mass using a Gaussian distribution centered on the Z mass plus a linear function. From the fit, the number of identified events containing a $Z \to e^+e^-$ decay, N_1^Z, is determined along with the number of background events in the

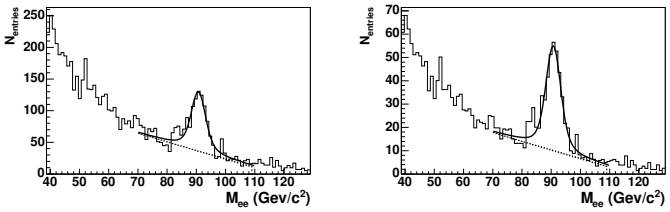

Fig. 2. Gaussian plus linear fit to the e^+e^- invariant mass distribution from a sample of $Z \rightarrow e^+e^-$ events, added to a background distribution corresponding to 60% of the peak area (see text). The histogram on the left corresponds to single-tagged events selected by signature *e25i* with an e^+e^- pair identified offline, while the histogram on the right corresponds to double-tagged events selected by *2e25i*.

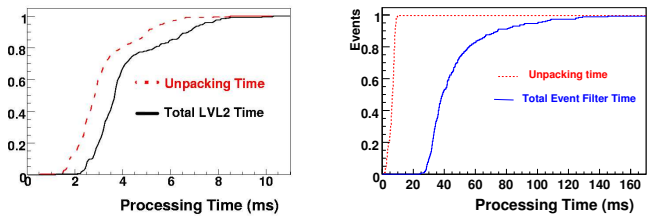

Fig. 3. Integrated distribution of the LVL2 (left) and EF (right) execution time per RoI extrapolated to a $8GHz$ or multi-core equivalent processor.

fit region, B_1. The same process is followed using a double-electron trigger with the same efficiency, such as *2e25i*. This results in the number of signal and background events N_2^Z and B_2. Figure 2 shows the fits to the single (double) electron signature on the left (right).

The number of $Z \rightarrow e^+e^-$ events tagged with the single and double triggers is given by

$$N_1^Z = \varepsilon_{rec}^Z(2\varepsilon_{trig} - \varepsilon_{trig}^2)N_0^Z + B_1 \quad (2)$$

and

$$N_2^Z = \varepsilon_{rec}^Z\varepsilon_{trig}^2 N_0^Z + B_2 \quad (3)$$

where N_0^Z is the true number of $Z \rightarrow e^+e^-$ in the data sample, ε_{rec}^Z is the efficiency for accurately reconstructing the Z mass peak offline, including the detector acceptance, and ε_{trig} is the efficiency. From equations 2 and 3, the trigger single-electron efficiency can be obtained as

$$\varepsilon_{trig} = 2\frac{N_2^Z - B_2}{N_1^Z + N_2^Z - B_1 - B_2} \quad (4)$$

The background contamination in the peak region is expected to be very small, but could constitute a systematic error on the measurement. To quantify this effect, invariant mass histograms obtained from QCD events were added to the e^+e^- histogram so that they would correspond to 5%, 20% or 60% of the histogram contents in the fitted region. The same efficiency was found, independently of the fraction of added background.

This method was tested on a $Z \rightarrow e^+e^-$ sample resulting in an efficiency of 87.0% for the particular set of cuts used in the *e25i* signature. The same value was found by counting simulated events selected by this signature.

Assuming an instantaneous luminosity of $10^{33}cm^{-2}s^{-1}$, for a $Z \rightarrow e^+e^-$ cross section of 1.515 nb, this leads to an estimated statistical uncertainty for the overall *e25i* efficiency of $\sim 3\%$ after ~ 1 hour of running at this luminosity.

E. Timing measurements

A constant effort is devoted to optimizing the time performance of the HLT. This section shows the time performance of LVL2 and the Event Filter for electron signatures. Figure 3 shows the integrated distributions of LVL2 (left) and EF [12] (right) execution times per RoI for a $8GHz$ or multi-core equivalent processor. The histograms can thus be read as the probability distributions that the reconstruction steps in LVL2 or the EF electron signatures will take less than a certain amount of time per RoI. The figure was produced using di-jet events with overlaped minimum-bias events corresponding to the design LHC luminosity of $10^{34}cm^{-2}s^{-1}$.

As can be seen from the figure, while the EF execution time is much shorter than the available time of ~ 1 s, the situation in LVL2 still needs some improvement. In the latter case, the average execution time is 5.8 ms per RoI, which is not negligible in comparison to the average available time of 10 ms.

The "unpacking", or data preparation time is also shown in the figure. It may be noticed that most of the time taken by LVL2 is spent in unpacking data. This is where most optimization efforts are being placed.

F. Performance measurements from testbeam data

The ATLAS combined test beam (CTB), which operated between May and November 2004, used beams produced by the SPS accelerator at CERN and included prototypes of the ID, LAr, Tilecal and Muon subdetector systems [18]. Events were selected either by using LVL1 trigger logic or using trigger signals produced by the SPS. The HLT software framework and data flow were used for the first time on real data, although not for event selection.

From the point of view of the electron and photon HLT signatures [17], the data produced during the CTB was used to study positron/pion separation at LVL2. The TRT was not used in the study. This allowed its use, together with other CTB-specific detectors, to select high purity positron and pion samples for analysis. Positron and pion samples of momentum 20 GeV and 50 GeV were selected. After this filtering, the fraction of pions in positron beams was less than 3×10^{-5} and 5.4×10^{-7} for the 20 GeV and 50 GeV beams, respectively. Conversely, the positron contamination fraction in pion beams was less than 8.3×10^{-4} and 1.6×10^{-3}. The samples were considered as pure positron and pion samples in further analysis.

The LVL2 single-electron signature performance and cut thresholds, as well as the pion fake rate, were studied using the filtered samples. The distributions of some of the quantities used for the selection of electrons are shown in figure 4 for

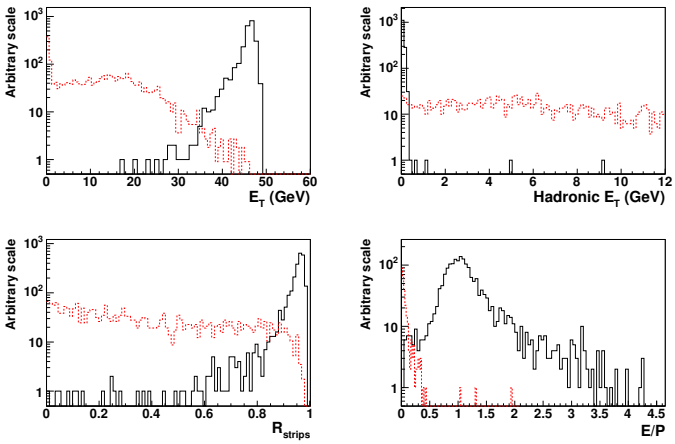

Fig. 4. Some quantities used for electron selection measured with the 50 GeV electron (in black) and pion (in red) beams. The left column shows the distributions found for each measured quantity, while the plots in the right column show the cut efficiency as the cut threshold on each quantity is varied. The quantities shown in the picture were defined in section IV.

TABLE VI

EFFICIENCY AND PION FAKE RATES OF LVL2 ELECTRON SIGNATURE FOR 20 GeV AND 50 GeV POSITRON AND PION TEST BEAM DATA.

	electron efficiency (%)		pion fake rate (%)	
	20 GeV	50 GeV	20 GeV	50 GeV
calorimeter	94.2 ± 0.5	96.1 ± 0.5	0.9 ± 0.2	0.4 ± 0.1
track matching	90.1 ± 0.7	91.8 ± 0.6	0.8 ± 0.1	0.2 ± 0.1

50 GeV electron (black) and pion (red) beams. The quantities shown in the picture were defined in section IV, The tracking algorithm used was found to have a track finding efficiency between 96% and 98% for positrons and pions of both beam energies. Some discriminating variables used in the *e25i* signature at LVL2, such as the angular differences between track and cluster, had little discriminating power in the context of the test beam, where the event geometry is fixed.

The trigger efficiency, obtained after optimization of the selection cuts, is shown in table VI.

VI. CONCLUSION

The LHC will start collecting data in 2007 and will provide the highest centre of mass collisions ever achieved in accelerator particle physics. The ATLAS experiment physics programme will cover a wide range of physics channels and is expected to contribute much to our knowledge of fundamental interactions.

ATLAS will need a very performing trigger system to reject vast amounts of background in a very challenging environment. An overview of the High Level Trigger signatures designed to select events containing high-p_T electrons and photons was given in the present paper.

Several studies of electron and photon signature performance were described, including efficiency and rate estimates with single-particle and physics-motivated simulated data, trigger timing, and tests performed on real data from the 2004 ATLAS combined test beam. Further work should be devoted to a few topics, such as the optimization of the timing performance.

Future work in this area must also include the preparations for detector and trigger comissioning, such as the necessary monitoring and calibration triggers. This work will build on what has been achieved already, to guarantee that the HLT electron and photon selection will fulfill its important role in the ATLAS experimental programme.

ACKNOWLEDGMENT

The authors would like to thank warmly the ATLAS TDAQ community for all the direct and indirect contributions to the work presented in this paper .

REFERENCES

[1] ATLAS Collaboration, *First-level Trigger Technical Design Report*, CERN/LHCC/98-14, 1998.
[2] ATLAS Collaboration, *ATLAS High-Level Trigger, Data Acquisition and Controls Technical Design Report*, CERN/LHCC/2003-022, 2003.
[3] ATLAS Collaboration, *ATLAS Detector and Physics Performance Technical Design Report*, CERN/LHCC/99-14 and CERN/LHCC/99-15, *ATLAS TDR* 1999.
[4] ATLAS Collaboration, *Inner Detector Technical Design Report*, CERN/LHCC/97-16, CERN/LHCC/97-17, 1997.
[5] ATLAS Collaboration, *Calorimeter Performance*, CERN/LHCC 96-40, 1996.
[6] ATLAS Muon Collaboration, *ATLAS Muon Spectrometer Technical Design Report*, CERN/LHCC 97-22, 1997.
[7] A. Anjos and others, *The Second Level Trigger of the ATLAS experiment at CERN's LHC*, ATL-COM-DAQ-2003-052, proceedings of the 2003 IEEE Nuclear Science Symposium And Medical Imaging Conference, Portland, Oregon, USA, 19-24 Oct 2003.
[8] G. Comune and others,*The Algorithm Steering and Trigger Decision mechanism of the ATLAS High Level Trigger*, ATL-DAQ-2003-031, Proceedings CHEP 2003, 24-28 Mar 2003, La Jolla, CA, USA, published in Nucl.Instrum.Methods Phys.Res., A 518 (2004)
[9] S. Armstrong and others, *An overview of Algorithms for the ATLAS High Level Trigger*, ATLAS-CONF-2003-003, Proceedings IEEE-NPSS Real Time Conference, 18-23 May 2003, Montréal, Québec, Canada, published in IEEE Trans.Nucl.Sci. 51 (2004) 367-374.
[10] C.Schiavi and others, *Fast Tracking for the Second Level Trigger of the ATLAS Experiment Using Silicon Detectors Data*, ATL-DAQ-CONF-2005-011, proceeedings of the 2004 IEEE Nuclear Science Symposium And Medical Imaging Conference, 16-22 October 2004, Rome, Italy.
[11] N.Konstantinidis and others, *Fast Tracking for the ATLAS LVL2 Trigger*, ATL-DAQ-CONF-2005-001, proceedings of the Computing in High Energy Physics and Nuclear Physics 2004 conference, Interlaken, Switzerland , 27 September - 01 October, 2004.
[12] C. Santamarina and others, *Implementation and Performance of the Seeded Reconstruction for the ATLAS Event Filter Selection Software*, ATL-DAQ-CONF-2005-032, Proceedings of the 14^{th} IEEE-NPSS Real Time Conference, 4-10 June 2005, Stockholm, Sweden.
[13] M.V. Gallas and others, *ATLAS Detector Simulation: Status and Outlook*, these proceedings.
[14] Geant4 Collaboration (S. Agostinelli and others), *GEANT4: A Simulation Toolkit*, Nucl.Instrum.Methods A 506 (2003), 250-303.
[15] T. Sjöstrand and others, Computer Phys. Commun. 135 (2001) 238 (LU TP 00-30, hep-ph/0010017).
[16] S. Brandt, *Data Analysis*, 3^{rd} edition, Springer Verlag, New York, 1999.
[17] M. Diaz Gomez, *Performance Studies of the ATLAS HLT Electron Trigger*, PhD Thesis, in preparation, expected Dec 2005.
[18] A. Anjos and others, *Deployment of the ATLAS High Level Trigger*, ATL-DAQ-CONF-2005-033, Proceedings of the 14^{th} IEEE-NPSS Real Time Conference, 4-10 June 2005, Stockholm, Sweden.